Design and synthesis of gas permeation membranes for extracorporeal membrane oxygenation (ECMO)

Maria Inês Bairos Teixeira Coelho

Supervisors: Dr. Mónica Cristina Faria Besteiro and Prof. Vasco Daniel Bigas Bonifácio

May 2022

Abstract:

Three groups of nonporous symmetric membranes were prepared by the solvent evaporation technique: pure polyurethane (PU) membranes, polyurethane-based membranes with tris(hydroxymethyl)aminomethane (TRIS), Congo red (CR) and methyl-beta-cyclodextrin (MBCD), and mixed matrix membranes (MMMs) incorporating Zn-NH_2-BDC and Cu-BTC metal organic frameworks (MOFs). The solvent used in the preparation of the casting solutions was dimethylformamide (DMF). Different total polymer/solvent and polyurethane/second reagent weight ratios were used across the different formulations.

All the membranes were examined by scanning electron microscopy (SEM), which revealed their nonporous, dense cross-section morphology. Energy-dispersive X-ray spectroscopy (EDS) was performed on the MMMs to confirm the presence of MOFs. The chemical nature of the membranes was characterized by Attenuated total reflection (ATR)–Fourier transform infrared (FTIR) spectroscopy. Tensile tests were performed on the pure polyurethane and polyurethane-based membranes to determine mechanical properties such as the Young's modulus, tensile strength, and elongation at break.

Single gas, oxygen (O_2) and carbon dioxide (CO_2) permeation studies were carried out by the constant volume method at 37 °C in an in-house built experimental set-up. The permeability coefficients obtained from the permeation curves ranged from 237 to 346 Barrer for CO_2 and 24 to 30 Barrer for O_2. The ranges obtained for the diffusion coefficients by the time-lag method were $1.4x10^{-6}$-$3.1x10^{-6}$ cm^2/s for CO_2 and $1.5x10^{-6}$-$2.6x10^{-6}$ cm^2/s for O_2, and the ranges obtained for the solubility coefficients were $114.5x10^{-4}$-$185.5x10^{-4}$ $cm^3/cm^3.cmHg$ for CO_2, and $11.4x10^{-4}$-$16.6x10^{-4}$ $cm^3/cm^3.cmHg$ for O_2.

Keywords: Membrane blood oxygenator; Gas permeation; Nonporous symmetric membranes; Bi-soft segment polyurethanes; Mixed matrix membranes; Time-lag.

1. Introduction

Extracorporeal membrane oxygenation (ECMO) is a form of cardiopulmonary bypass that was first developed in the 1970s. Nowadays, this therapy is commonly used during cardiopulmonary surgeries, as bridge-to-transplant support for cardiac and lung transplants and lung resections, as well as during recovery in intensive care units. In the ECMO circuit, the patient's deoxygenated blood is first drained and pumped through a membrane blood oxygenator (MBO), which removes the carbon dioxide from the blood (CO_2) and enriches it in oxygen (O_2). The oxygenated blood is then warmed up by a heat exchanger and returned to the patient [1,2].

Despite a long history of extensive use and continuous development, MBOs still need improvement in various aspects, such as the conditions for blood circulation, equipment design and membrane/blood interactions. The progress in the performance of MBOs is closely tied to the development of novel gas permeation membranes, since this is where the gas exchange occurs within the oxygenator. The two main requirements these membranes must fulfill are:

(i) Hemocompatibility,

(ii) Suitable gas permeation properties, ensuring the delivery of approximately 250 cm^3 (STP)/min of O_2 and removal of 200 cm^3 (STP)/min of CO_2, at blood flow rates of 2–4 L/min [3].

The pursuit of increasingly efficient gas exchange membranes, which consequently require smaller membrane areas, lower priming volumes and lower blood flows, could lead to a new generation of smaller, more practical MBO systems. Therefore, over the last decades, membranes have been produced in a multitude of different polymers and configurations.

The first membranes used in oxygenators were composed of silicone rubber, which exhibits very high O_2 and CO_2 permeation rates and reasonable hemocompatibility. In an attempt to further enhance the blood compatibility, other materials such as polypropylene (PP), polymethylpentene (PMP), polyethylene (PE), polyvinylidene fluoride (PVDF) have been investigated for gas permeation membranes [4]. Nonetheless, these materials do not exhibit permeation rates as high as silicone rubber and continue to be associated to complications such as plasma leakage, bleeding, and myocardial and brain infarction caused by thrombus formation [5,6].

An alternative material that has shown great potential is polyurethane (PU), with distinguished characteristics such as high bio- and hemocompatibility, as well as good fatigue resistance, tear resistance and mechanical strength [7]. These properties make PU suitable for a wide variety of biomedical applications.

Polyurethanes typically exhibit two phases: hard segment (HS) enriched domains, dispersed in a soft segment (SS) matrix. The soft, amorphous segments provide thermoplastic elastomeric character, while the hard, crystalline segments increase mechanical strength. Additionally, a second type of SS can be introduced into the structure of polyurethane membranes, further increasing its versatility. Research by de Pinho's group show that parameters like the type, length and molecular weight of the segments, hard-to-soft segment ratio and surface functionalization can be finetuned during synthesis in order to obtain improved permeation properties [8,9].

Therefore, several bi-soft segment poly(urethane urea) (PUU) membranes have been studied for membrane oxygenator applications, each containing different second SS's, such as poly(butadienediol) (PBDO), poly(dimethylsiloxane) (PDMS) and polycaprolactone (PCL).

The gas exchange properties of the PUR/PBDO and PUR/PDMS bi-soft segment membranes were studied by Zhao [10] and by de Queiroz et al. [11], respectively. Despite having satisfactory gas permeation properties, results showed that the hemocompatibility of these types of membranes was limited. This led to the introduction of polycaprolactone as a second SS which has shown to have great blood compatibility. However, studies by Eusebio et al. [12] and Faria et al. [13] showed that the O_2 permeability for this type of membrane remained below the desirable threshold for MBOs, suggesting that additional investigation is needed to optimize the permeation properties of this type of membrane.

2. Experimental

2.1. Materials

All of the membranes in this work were prepared using a poly(propylene oxide) (PPO) based polyurethane prepolymer (PU) containing three isocyanate terminal groups and a molecular weight (MW) of approximately 3500 Da. This prepolymer was supplied by Fabrires - Produtos Químicos S.A. (Vendas Novas, Portugal). The solvent used was dimethylformamide (DMF) (p.a. grade, 99.8%) provided by Panreac (Barcelona, Spain).

In addition to the polyurethane, three reagents were used: tris(hydroxymethyl)aminomethane (TRIS), Congo red (CR), and methyl-beta-cyclodextrin (MBCD). TRIS (purity ≥ 99.8%) was provided by Sigma-Aldrich (St. Louis, MO, USA). CR (purity > 98.0%) was provided by Tokyo Chemical Industry Co., Ltd. (Tokyo, Japan). MBCD, with a MW of 1303.3 Da, was provided by Sigma-Aldrich (St. Louis, MO, USA).

Lastly, two metal-organic frameworks (MOFs) were used, Zn-NH_2-BDC (also referred to as IRMOF-3) and Cu-BTC (alternatively known as HKUST-1), which were synthesized according to previously reported methods [14]. Both MOFs were kindly provided by Dr. Anirban Karmakar from the Center of Structural Chemistry at Instituto Superior Técnico.

The gas permeation experiments were performed using carbon dioxide (purity ≥ 99.98%) and oxygen (purity ≥ 99.5%), both provided by Air Liquide (Lisbon, Portugal).

2.2. Membrane Synthesis

Three groups of polyurethane-based membranes were prepared by the solvent evaporation technique: pure polyurethane membranes, polyurethane-based membranes, and mixed matrix membranes (MMMs). The pure polyurethane membranes (group 1), named PU and PU-s, were obtained from casting solutions of polyurethane (PU) with and without solvent, respectively. The polyurethane-based membranes (group 2), designated by PU/TRIS, PU/CR and PU/MBCD, were prepared from casting solutions of PU and solvent with TRIS, CR and MBCD, respectively. Lastly, the MMMs, named PU/Zn-NH2-BDC, PU/Cu-BTC-0.1 and PU/Cu-BTC-1.0, were synthesized by incorporating Zn-NH2-BDC and Cu-BTC MOFs into casting solutions of PU and solvent. The solvent used in all the formulations was dimethylformamide (DMF). The polymer to solvent ratios used were 65/35 for the PU-s and PU based membranes, and 90/10 for the MMMs. The polyurethane to second reagent ratios used were 99.2/0.8 for PU/TRIS, 99.6/0.4 for PU/CR and PU/MBCD, 99.9/0.1 for PU/Zn-NH2-BDC and PU/Cu-BTC-0.1, and 99/1 for PU/Cu-BTC-1.0.

Each casting solution was subjected to 2 hours of magnetic agitation and 10 minutes in an ultrasound bath, before being cast onto glass plates using a 250 µm casting knife. Then, the membranes were left to cure at room temperature for 24 to 48 hours and, finally, they were detached from the glass plates in a deionized water bath.

2.3. Characterization

All the synthesized membranes were observed by Scanning Electron Microscopy (SEM) using a Thermo Scientific™ Phenom™ ProX G6 desktop SEM (Waltham, MA, USA). For this observation, samples of the membrane were mounted on a stub and sputter-coated with gold before being observed. For each membrane, pictures of the cross-section, top surface and, in some cases, bottom surface were taken. The average thickness of each membrane was determined from measurements on the SEM images of the cross-sections. Additionally, energy-dispersive X-Ray spectroscopy (EDS) was used to detect the presence of metallic elements in the membranes containing MOFs.

Attenuated Total Reflectance - Fourier Transform Infrared (ATR – FTIR) spectroscopy was used to analyze the active layer of each polyurethane-based membrane. The equipment used was a Nicolet 5700 FT-IR spectrometer (Thermo Electron Scientific Instruments, Madison, WI, USA) with a Golden Gate MKII ATR accessory with a Ge crystal (Graseby Specac, Smyrna; sampling depth: 0.2–1.1 µm at 4000–400 cm-1). FTIR spectra were obtained from one sample of each composition by averaging 264 scans with a resolution of 4cm^{-1}, and processed using the OMNIC™ software (Thermo Fisher Scientific, Waltham, MA, USA).

Uniaxial tensile tests were performed on the pure PU and PU-based membranes in cooperation with Dr. Sérgio Gonçalves in the Laboratory of Tissue Biomechanics at Instituto Superior Técnico, using an Instron® 5544 universal testing machine (Norwood, MA, USA) coupled with an Instron® model 2663-822 standard video extensometer (Norwood, MA, USA), and a load cell of 100N. The tests were executed on specimens with a gauge length of 60mm that were cut from pre-cast membranes using a 3D-printed cutting cast. Each specimen was tested until rupture, at ambient conditions, with a uniform elongation rate of 15mm/min (0.0041 s^{-1}) [15]. The evolution of the extension, load and video axial strain over time were recorded by a computer using the Instron® Blue Hill version 3 software (Norwood, MA, USA). Only specimens which ruptured in the neck region were selected for further analysis.

2.4. Gas permeation Set-up and Tests

The gas permeation properties of the PU membranes were determined by the constant volume method using the set-up shown in Figure 1, which was developed by Eusébio [16] and optimized by Pon [17]. This method studies the gas flux through a membrane, by the application of gas at constant pressure to the feed side of the membrane, and the subsequent measurement of the variation of pressure in the receiving chamber (of constant volume) as a function of time.

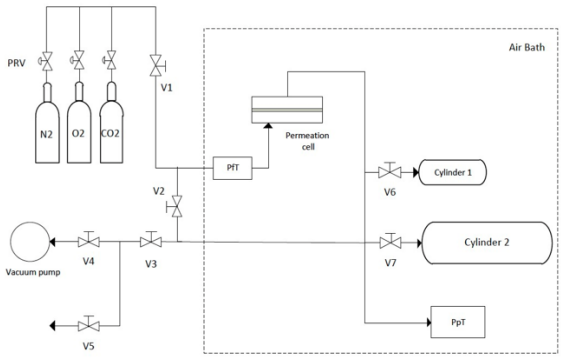

Figure 1. Schematic representation of the gas permeation set-up [43].

The permeation cell consists of two detachable flat plates made of stainless steel. Between the plates, there is a porous support with an effective surface area of 9.62 cm^2, on which a membrane sample is placed to be tested.

The feed gas cylinder, coupled to a pressure regulating valve (PRV), is connected to the feed side of the permeation cell through a valve (V1) and a Setra model 205-2 (Boxborough, MA, USA) feed pressure sensor (PfT). The receiving chamber on the permeate side of the cell is made up of two cylinders of different sizes, cylinder 1 with 12.6 ± 0.1 cm^3 and cylinder 2 with 167.2 ± 0.2 cm^3, connected through valves V6 and V7 respectively, and tubing with a volume of 13.5 ± 0.01 cm^3. The total volume of the receiving chamber is 193.3 ± 0.3cm^3. Connected to the permeate side is a Paroscientific Inc. model 6100A-CE (Redmond, WA, USA) permeate pressure transmitter (PpT) which, in turn, is connected to a Paroscientific Inc. model 710 display unit, and to a computer. The computer automatically records the permeate pressure as a function of time using the Digiquartz Interactive DQ13 ® version 1.0.1.0 software from Paroscientific Inc.

Both sides of the permeation set-up are linked through a series of valves (V2 to V5) to an Edwards model E2M2 vacuum pump (Burgess Hill, UK) and to the atmosphere. Lastly, the connections between the components of the system were made using Hoke® stainless steel 316 tubes with 1/8-inch outer diameter, Hoke® 3700 series needle valves, and Gyrolok® tube fittings of several materials (stainless steel, titanium and brass).

The set-up is installed inside a glass door refrigerator (wine cellar) that functions as a thermostatic air bath. The temperature inside the air bath is homogenized using a Hart Scientific model 2100 temperature controller (Everett, WA, USA) connected to a heater and two fans, and to a platinum resistance thermometer.

Before beginning the measurements, the system is degassed and thermostated until the temperature stabilizes at approximately 37ºC ± 0.3. Then, one single gas is fed (either CO_2 or O_2) at feed

pressures between 1.5 and 4 bar. The permeate pressure, detected by the PpT sensor in the receiving chamber is recorded as a function of time.

The total volume of the receiving chamber can be tailored to the permeance of the measured gas through the membrane sample, optimizing the accuracy of the measurements. In permeation measurements using carbon dioxide, only valve V6 was kept open making the total receiving volume 26.1 cm^3, while for oxygen, both valves remained closed, corresponding to a receiving volume of 13.5 cm^3.

2.5. Theory

2.5.1. Solution-Diffusion model

When a pressure difference is applied across a dense membrane, it acts as the driving force for the transport of gas, a process which is commonly described by the solution-diffusion model. In this model, the permeability, P, of a gas through a membrane is controlled by its solubility coefficient, S, and diffusion coefficient, D[18]:

$$\mathrm{P} = \mathrm{SD} \tag{1}$$

In the steady state, the unidimensional diffusive flux is described by the Fick's first law of diffusion:

$$\mathrm{J_i} = -\mathrm{D_i}\frac{\mathrm{dC_i}}{\mathrm{dx}} \tag{2}$$

where $\mathrm{J_i}$ is the flux of species i in the x direction and is proportional to the concentration gradient $\frac{\mathrm{dC_i}}{\mathrm{dx}}$, $\mathrm{C_i}$ is the concentration of species i in the membrane, and $\mathrm{D_i}$ is a proportionality constant defined as the diffusion coefficient, which is independent from the concentration at low pressure ranges [19].

The integration of Fick's first law across the total thickness, ℓ, of the membrane gives:

$$\mathrm{J_i} = \frac{\mathrm{D_i}}{\ell}(\mathrm{C_{i0}} - \mathrm{C_{i\ell}}) \tag{3}$$

where $\mathrm{C_{i0}}$ and $\mathrm{C_{i\ell}}$ are the concentrations of species i in the membrane on the feed side and permeate side respectively.

In elastomers, the solubility of gases tends to be very low and can be described by Henry's Law:

$$\mathrm{C} = \mathrm{Sp} \tag{4}$$

where C is the concentration inside the polymer and is proportional to the applied pressure, p [20].

By applying Henry's Law, the relations below can be established:

$$\mathrm{S_i} = \frac{\mathrm{C_{i0}}}{\mathrm{p_f}} = \frac{\mathrm{C_{i\ell}}}{\mathrm{p_p}} \tag{5}$$

where $\mathrm{S_i}$ is the solubility coefficient of species i, $\mathrm{p_f}$ is the pressure on the feed side and $\mathrm{p_p}$ is the pressure on the permeate side.

By combining expressions (3) and (5), the following expression is obtained:

$$\mathrm{J_i} = \frac{\mathrm{D_i S_i}}{\ell}(\mathrm{p_f} - \mathrm{p_p}) \tag{6}$$

Equation (1) gives us that the product $\mathrm{D_i S_i}$ is equal to the permeability coefficient of species i, $\mathrm{P_i}$, and thus, expression (6) can be written as follows:

$$\mathrm{J_i} = \frac{\mathrm{P_i}}{\ell}(\mathrm{p_f} - \mathrm{p_p}) \tag{7}$$

The permeability coefficient is commonly expressed in Barrer, with:

$$1\ \mathrm{Barrer} = 10^{-10}\left(\frac{\mathrm{cm^3(STP)cm}}{\mathrm{cm^2 s\ cmHg}}\right)$$

When the thickness is difficult to determine, the pressure normalized flux or permeance may be used instead:

$$\mathrm{Perm} = \frac{\mathrm{P_i}}{\ell} \tag{8}$$

2.5.2. Time-lag method

The mass balance of the unidimensional diffusive transport of species i across a nonporous polymeric membrane in the transient state is given by:

$$-\frac{\mathrm{dC_i}}{\mathrm{dt}} = \frac{\mathrm{dJ_i}}{\mathrm{dx}} \tag{9}$$

By combining this expression with Fick's First Law from equation (2), Fick's Second Law is obtained:

$$\frac{\mathrm{dC_i}}{\mathrm{dt}} = \mathrm{D_i}\frac{\mathrm{d^2C_i}}{\mathrm{dx^2}} \tag{10}$$

In a system where the membrane is initially free of diffusing species, the following initial and boundary conditions can be considered:

$$\mathrm{C_i}(\mathrm{x}, 0) = 0 \tag{11.a}$$

$$\mathrm{C_i}(0, \mathrm{t}) = \mathrm{C_{i0}} \tag{11.b}$$

$$\mathrm{C_i}(\ell, \mathrm{t}) = \mathrm{C_{i\ell}} \approx 0 \tag{11.c}$$

meaning that the upstream concentration, $\mathrm{C_{i0}}$, remains constant and, in comparison, the downstream concentration, $\mathrm{C_{i\ell}}$, is negligible. The solution of equation (10) is obtained by satisfying the boundary conditions listed above, and either through Laplace transform or separation of variables [21]:

$$C_i = C_{i0}\left(1 - \frac{x}{\ell}\right) + \frac{2C_{i0}}{\ell} \times \sum_{n=1}^{\infty} \frac{1}{n} \sin\left(\frac{n\pi x}{\ell}\right) \exp\left(-\frac{D_i n^2 \pi^2 t}{\ell^2}\right) \tag{12}$$

The diffusive flux, J_i, results from substituting equation (12) in Fick's First Law:

$$J_i(x,t) = \frac{D_i C_{i0}}{\ell} + \frac{2D_i C_{i0}}{\ell} \times \sum_{n=1}^{\infty} \cos\left(\frac{n\pi x}{\ell}\right) \exp\left(-\frac{D_i n^2 \pi^2 t}{\ell^2}\right) \tag{13}$$

where the first and second terms represent the steady state and transient state contributions of the flux, respectively. This expression is a function of time, t, and displacement in the direction of diffusion, x, which can easily be solved for the fluxes entering (x = 0) and leaving ($x = l$) the membrane.

By setting $x = \ell$ in equation (13) and then integrating it with respect to time, an expression for the permeate pressure can then be obtained:

$$p_p(t) = \frac{AD_i p_f}{V\ell}\left[t - \frac{\ell^2}{6D_i} + \frac{2\ell^2}{\pi^2 D_i} \times \sum_{n=1}^{\infty} \frac{(-1)^{n+1}}{n^2} \exp\left(-\frac{D_i n^2 \pi^2 t}{\ell^2}\right)\right] \tag{14}$$

where A is the area of the cross-section (perpendicular to the direction of diffusion) through which the gas permeates, and V is the volume of the receiving chamber. The transient term of equation (16) can be reduced to zero by calculating the limit as $t \to \infty$, resulting in the following expression for the permeate pressure:

$$\lim_{t\to\infty} p_p(t) = \frac{AD_i p_f}{V\ell}\left[t - \frac{\ell^2}{6D_i}\right] \tag{15}$$

In the plot of the permeate pressure versus time, the time value at which the steady state asymptote intercepts the time axis is defined as the time lag, t_{lag}. An example of the application of this method is shown in Figure 2.

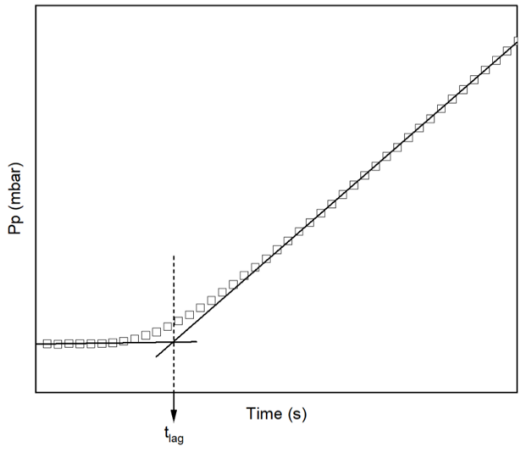

Figure 2. Plot of the permeate pressure versus time showing the time lag value, t_{lag}, at the interception of the x axis (p_p=0) and the steady state asymptote.

Knowing the time lag value and the membrane thickness, the diffusion coefficient can be obtained by:

$$t_{lag} = \frac{\ell^2}{6D_i} \tag{16}$$

3. Results and Discussion

3.1. Scanning Electron Microscopy

The cross-section morphology of each membrane was characterized by scanning electron microscopy (SEM). Figure 3 shows the SEM images of the top surface and cross-section of the pure polyurethane membranes.

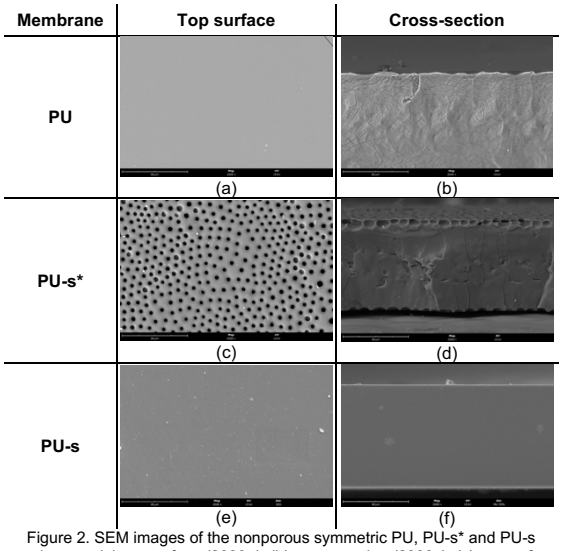

Figure 2. SEM images of the nonporous symmetric PU, PU-s* and PU-s membranes: (a) top surface (2000×), (b) cross-section (2000x), (c) top surface of PU-s* (2000x), (d) cross-section of the of PU-s* (2000x); (e) top surface of PU-s (2000x), (d) cross-section of PU-s (2000x).

As expected, the PU membrane appears to be completely dense with no observable porosity. However, two different structures were observed for the pure PU membranes prepared with 35% solvent, which were designated by PU-s* and PU-s. The PU-s* membrane exhibits a dense, almost nonporous core, with porous top and bottom surfaces. The PU-s membrane, on the other hand, appears to be entirely dense with no visible pores on the surfaces or core. Both PU-s* and PU-s membranes were synthesized using the same materials, polymer to solvent ratio, agitation time and curing time. Nevertheless, because they were prepared on different days, the variation in the composition of the atmosphere and of the room temperature could have affected the solvent evaporation process, thus resulting in different structures. Because the structure observed in PU-s* was not reproducible, only the PU-s membrane could be further investigated in the remainder of this work.

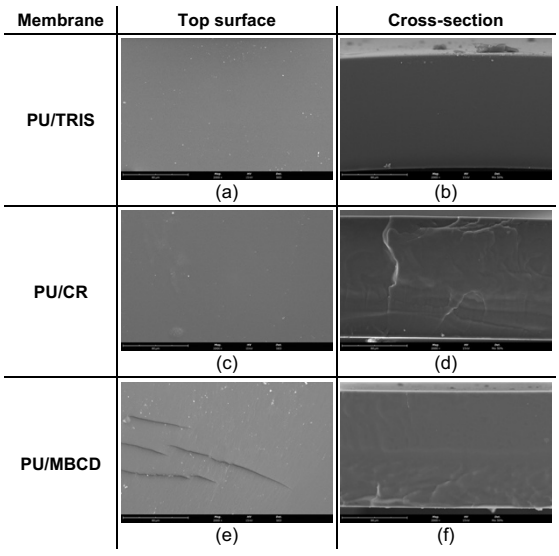

Figure 3. SEM images of the nonporous symmetric PU/TRIS, PU/CR and PU/MBCD membranes: (a)top surface of PU/TRIS (2000x), (b)cross-section of the of PU/TRIS (2000x); (c)top surface of PU/CR (2000x), (d)cross-section of PU/CR (2000x); (e)top surface of PU/MBCD.

SEM images of the top surfaces and cross-sections of the polyurethane-based membranes from group 2 are presented in Figure 4. All the polyurethane-based membranes have a dense, homogenous appearance with no discernable porosity. The addition of TRIS, CR and MBCD does not seem to have any influence on membrane morphology when compared to the dense PU-s membrane, which was synthesized using an analogous polymer to solvent ratio.

SEM micrographs of the top surface and cross-section of the MMMs from group 3 are shown in Figure 5. All the MMMs exhibit dense matrices with no observable pores, similarly to the pure PU membrane. The cross-section images of the PU/Zn-NH_2-BDC and PU/Cu-BTC-1.0 membranes revealed the existence of small masses, presumably Zn-NH_2-BDC and Cu-BTC respectively, distributed throughout the polyurethane matrix. No fillers were found in the cross-section images of the PU/Cu-BTC-0.1 membrane, likely because the proportion of filler is so small that, coincidentally, no Cu-BTC was intercepted by the specific cross-sectional plane obtained during sample preparation. The surfaces of each sample were examined using a backscattered electron (BSE) SEM signal, which is highly sensitive to differences in atomic number. The higher the material's atomic number, the brighter it appears on the image. All three MMM samples contained discernable brighter, diffuse spots dispersed through their surfaces, confirming the localized presence of MOFs within the membranes.

The observable cracks on the surfaces of the PU/MBCD, PU/Cu-BTC-0.1 and PU/Cu-BTC-1.0 membranes were likely created during the removal of the membranes from the glass plates or during the sputtering of the membrane samples. In any case, the fissures are not deep as they are not visible in any of the cross-section images.

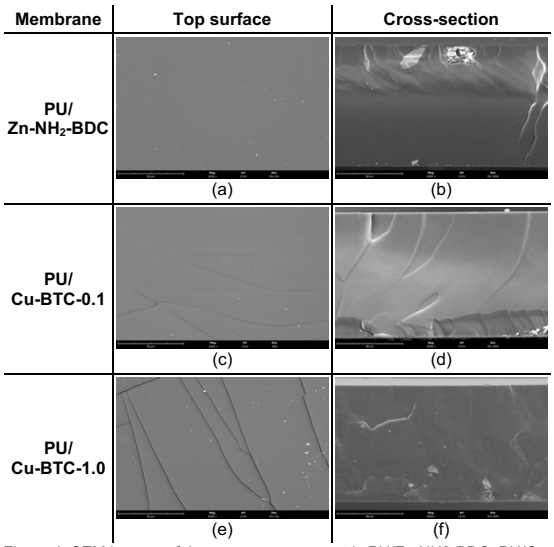

Figure 4. SEM images of the nonporous symmetric PU/Zn-NH2-BDC, PU/Cu-BTC-0.1 and PU/Cu-BTC-1.0 membranes: (a) top surface of PU/Zn-NH2-BDC (2000x), (b) cross-section of the of PU/Zn-NH2-BDC (2000x); (c) top surface of PU/Cu-BTC-0.1 (2000x), (d) cross-section of PU/Cu-BTC-0.1 (2000x); (e) top surface of PU/Cu-BTC-1.0 (2000x), (f) cross-section of PU/Cu-BTC-1.0 (2000x).

The total thickness (ℓ) of each studied membrane was measured on five points of the cross-section SEM micrographs. Table 1 shows the average values and respective standard deviations obtained for each composition. The pure PU membrane synthesized with no solvent exhibits the highest thickness, while the PU-s membrane produced with 35 wt% solvent has the lowest thickness, suggesting that the introduction of solvent reduces the thickness of the membrane. All PU-based membranes and MMMs, from groups 2 and 3 respectively, exhibit intermediate values of thickness. Moreover, on average, the PU-based membranes synthesized with 35 wt% solvent are thinner than the MMMs prepared with 10 wt% solvent, which supports the premise that casting solutions with higher solvent content result in membranes with lower thickness.

Table 1. Average thickness (l) and respective standard deviation of the nonporous symmetric PU membranes from groups 1, 2 and 3, obtained from the SEM cross-sectional images.

	Membrane	Thickness, ℓ (μm)
Group 1	PU	181 ± 0.9
	PU-s*	111 ± 0.6
	PU-s	125 ± 0.3
Group 2	PU/TRIS	137 ± 1.0
	PU/CR	149 ± 0.3
	PU/MBCD	144 ± 0.4
Group 3	PU/ Zn-NH_2-BDC	152 ± 0.9
	PU/Cu-BTC-0.1	154 ± 0.9
	PU/Cu-BTC-1.0	143 ± 0.7

3.2. Energy dispersive X-ray spectroscopy

During the SEM session (and using the same equipment), energy-dispersive X-ray spectroscopy (EDS) was performed on the samples of the membranes containing MOFs (group 3), to analyze the composition of the masses observed in their cross-sections. Since no fillers could be distinguished in the cross-section of the PU/Cu-BTC-0.1 membrane, only the analysis of the PU/Zn-NH_2-BDC and PU/Cu-BTC-1.0 compositions provided useful information.

The EDS spectrum obtained for the PU/Zn-NH_2-BDC membrane sample is displayed in Figure 6. The data shows that the mass visible in the cross-section of the membrane contained a significant amount of zinc (Zn), strongly suggesting that they were in fact Zn-NH_2-BDC particles.

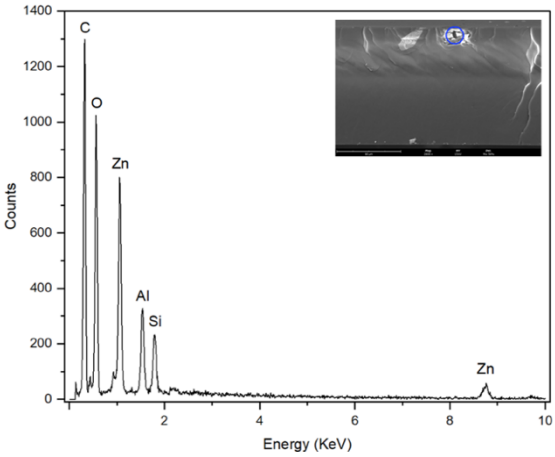

Figure 5. Energy-dispersive X-ray spectrum of the PU/Zn-NH_2-BDC membrane. The inset image shows the region of the sample that was analyzed (circled in blue).

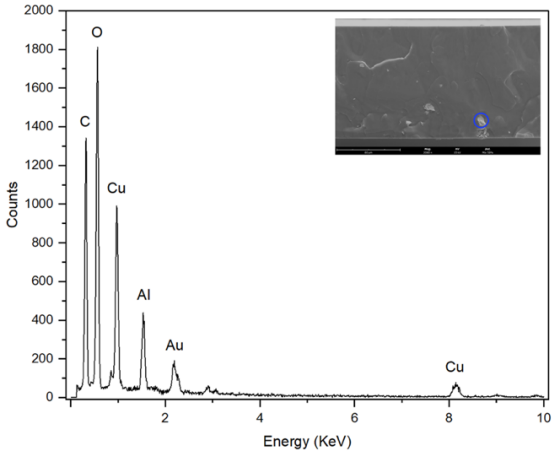

Figure 6. Energy-dispersive X-ray spectrum of the PU/Cu-BTC-1.0 membrane. The inset image shows the region of the sample that was analyzed (circled in blue).

Similarly, the EDS spectrum presented in Figure 7 for the specks observed in the cross-section of the PU/Cu-BTC-1.0 membrane, exhibits a peak for copper (Cu), confirming that the mass is most likely a Cu-BTC particle. The high amounts of carbon (C) and oxygen (O) found in both spectra were expected, as these elements constitute a large part of the PU's chemical structure. The small amounts of gold (Au) and aluminum (Al) detected are due, respectively, to the support material and sputter coating used in the preparation of the SEM samples. Finally, the vestigial traces of silicon (Si) observed are most likely due to impurities.

3.3. Attenuated Total Reflectance – Fourier Transform Infrared Spectroscopy

The active layers of all the studied membranes and of the PU prepolymer were analyzed via attenuated total reflectance – Fourier transform infrared spectroscopy (ATR-FTIR). Figures 8 and 9 show the ATR-FTIR spectra (4000-500 cm^{-1}) obtained for the pure polyurethane and polyurethane-based membranes, and for the mixed matrix membranes, respectively. The spectrum for the PU prepolymer is displayed for reference in both figures.

Several bands can be identified on the ATR-FTIR spectra of the PU, PU-s, PU/TRIS, PU/CR and PU/MBCD membranes as well as the PU prepolymer: the urethane/urea carbonyl stretching region (υC=O) centered at approximately 1725 cm^{-1}, and both urethane C-O-C and ether aliphatic C-O-C asymmetric stretching regions (υ_{as}COC) at about 1085 cm^{-1} [8,9]. However, while all membranes showed the urethane/urea carbonyl stretching band (ca. 1730 cm^{-1}), none exhibited a peak for the asymmetric isocyanate stretching mode (υ_{as}NCO) centered at 2278 cm^{-1}, which is clearly present in the PU prepolymer spectrum (top of Figure 7) [9]. This indicates that all the isocyanate groups are likely to have reacted with the functional groups of other components present in the PU-based membranes (TRIS, CR and MBCD), and with the water present in ambient air (particularly in the PU and PU-s membranes). Consequently, when the reaction occurs with the amine groups, urethane and urea linkages are formed.

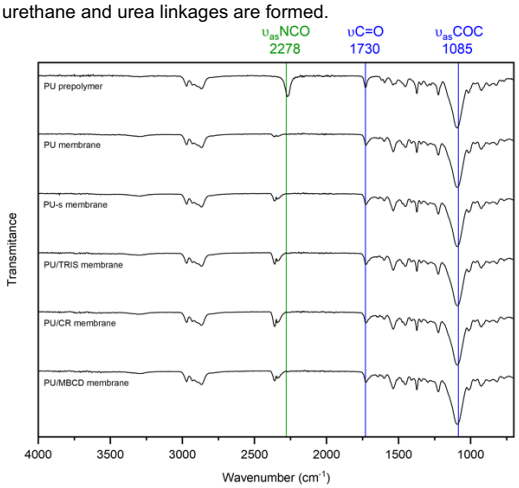

Figure 7. ATR-FTIR spectra of the uncured PU prepolymer and the PU, PU-s, PU/TRIS, PU/CR and PU/MBCD membranes.

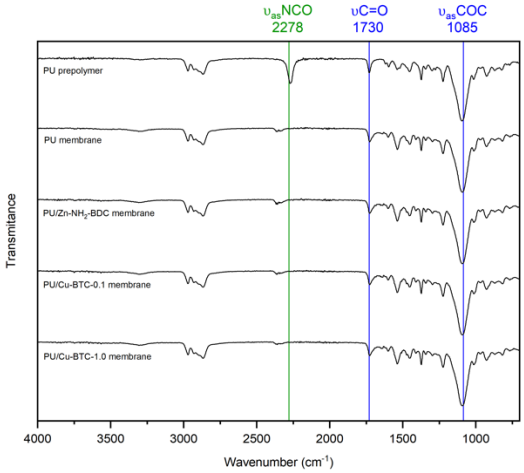

Figure 8. ATR-FTIR spectra of the uncured PU prepolymer and of the PU, PU/Zn-NH2-BDC, PU/Cu-BTC-0.1 and PU/Cu-BTC-1.0 membranes.

It is important to note that the peaks observed at about 2300-2400 cm^{-1} are most likely due to a growing concentration of respiratory CO_2 in the room where the FTIR characterization occurred [22].

All the same observations made for the spectra of the PU-based membranes can also be made for the spectra obtained for the MMMs, shown in Figure 8, although, in this case, it is expected that the reactions occur mainly among the PU prepolymer chains themselves or with the water from the atmosphere, rather than between the prepolymer and the MOFs.

3.4. Mechanical Tests

To determine and compare the mechanical properties, uniaxial tensile tests were performed on all the pure polyurethane and polyurethane-based membranes. Figure 10 shows the engineering stress-strain diagrams obtained for five selected specimens of each tested formulation. All membranes display similar stress-strain behaviors, typical of elastomers, with the initial slope of the curves steadily decreasing as the strain increases, finally reaching a steady slope region. None of the curves present a well-defined yield point, and no clear transition between elastic and plastic regimes can be observed. This is characteristic of rubber-like materials which are known to exhibit high elasticity.

The average values of the Young's modulus (E), tensile strength and elongation at break obtained for each tested formulation are presented in Table 2.

Table 2. Mechanical properties of the pure polyurethane and polyurethane-based membranes, obtained from the tensile tests.

Membrane		E (MPa)	Tensile Strength (MPa)	Elongation at Break (%)
Group 1	PU	8.0 ± 0.4	2.7 ± 0.4	94.65 ± 20.80
	PU-s	2.6 ± 0.1	1.5 ± 0.1	100.31 ± 7.76
Group 2	PU/TRIS	3.0 ± 0.2	1.4 ± 0.1	78.70 ± 15.79
	PU/CR	2.3 ± 0.1	1.5 ± 0.1	116.35 ± 14.29
	PU/MBCD	4.2 ± 0.1	2.0 ± 0.3	103.99 ± 19.28

The Young's modulus is given by the initial slope of the stress-strain curve and is a measure of the material's stiffness. Generally, elastomers such as polyurethanes are said to be soft materials which sustain large deformations under relatively small forces, as opposed to glassy polymers which are stiffer and require large forces to reach small deformations [20]. All the E values shown in Table 2 have the same order of magnitude and low standard deviations. Although the values are relatively low, some differences can be observed among the various compositions. The PU membrane exhibits the highest Young's modulus, followed by the PU/MBCD membrane and finally, the PU-s, PU/TRIS and PU/CR compositions, which present the lowest values. All the same tendencies can be observed for the tensile strength, which is the maximum stress that can be applied to a material. In this case, it coincides with the stress at failure.

Higher degrees of cross-linking in elastomers lead to higher stiffness (and Young's modulus) in deformation. It is possible that the use of solvent in the synthesis of the membranes may have had an impact on the packing of the polymer chains during the cure, causing lower degrees of entanglement and cross-linking, and consequently, lower values of E and UTS, than in the PU membrane synthesized without solvent.

Another parameter that was obtained from the stress-strain diagram is the elongation at break, or the amount of strain (%) under which the material ruptures. The highest average value was found for the PU/CR composition at 116%. The PU, PU-s and PU/MBCD membranes ruptured at intermediate elongations of 94%, 100% and 103% respectively. Finally, the PU/TRIS specimens ruptured at a significantly lower average elongation of 78%. A material is said to be brittle if it breaks under a small deformation (about 1 to 2%), or tough if it breaks for big deformations. The relatively high elongations observed for the tested membranes are coherent with the behavior observed in elastomers, which are typically tough [20].

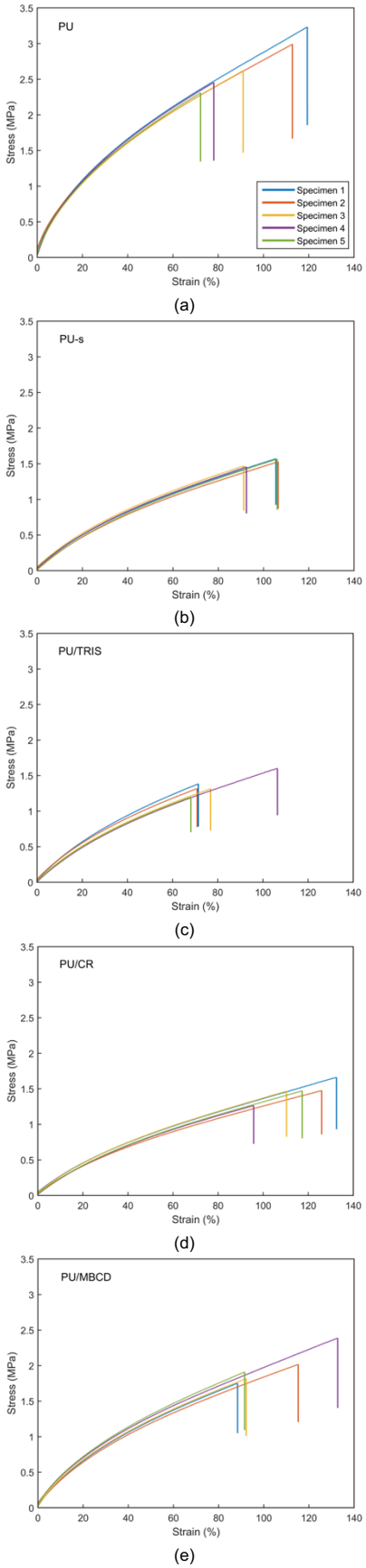

Figure 9. Stress-strain curves obtained for the pure polyurethane and polyurethane-based membranes: (a) PU, (b) PU-s, (c) PU/TRIS, (d) PU/CR and (e) PU/MBCD. Multiple specimens are shown for each composition.

3.5. Gas permeation measurements

3.5.1. Volumetric flux as a function of the transmembrane pressure

A series of gas permeation experiments were conducted on all the synthesized membranes using the set-up described in section 2.4. In each test, pure CO_2 or O_2 gas was fed through a 9.62cm^2 membrane sample and the variation of permeate pressure in the receiving chamber was recorded as a function of time.

Figure 11 shows an example of the CO_2 and O_2 permeation curves, recorded at a feed pressure (p_f) of 3 bar, for the PU-s membranes. Similar curves were obtained for all the compositions at multiple feed pressures, varying between 1.5 and 4 bar.

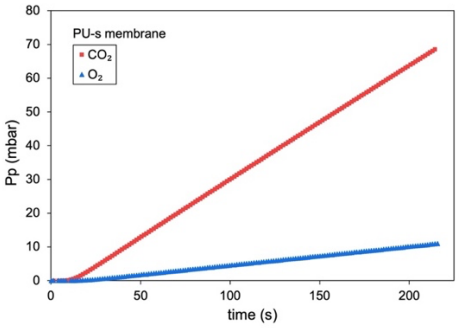

Figure 10. Permeate pressure (p_P) vs. time (t) of CO_2 and O_2 gases (p_F=3 bar) for the PU-s membrane.

Two distinct regions could be identified in all the permeation curves recorded. The first region, usually under 40s, corresponds to the transient state, in which the permeate pressure remains constant through time. The second region, known as the steady state region, is marked by a gradual increase of the permeate pressure with time. In general, the slope of the steady state region of the curves is steeper for CO_2 than for O_2, which is typical in this type of membrane.

The curves obtained from permeation experiments are commonly used to determine the volumetric flux, J, of gas through the studied membrane, by the following expression:

$$J = \frac{dp_p}{dt} \cdot \frac{V_s T_{STP}}{T p_{STP}} \cdot \frac{1}{A} \quad (1)$$

where $\frac{dp_p}{dt}$ is the slope of the steady state region of the permeation curve, V_s is the receiving chamber's volume, T is the absolute temperature at which the tests were carried out, and T_{STP} and p_{STP} are the temperature and pressure in STP conditions, which correspond to 273.15 K and 1 atm respectively, and A is the effective membrane area [12].

Since the permeation curves of CO_2 and O_2 were obtained at several feed pressures for each membrane sample, it was possible to plot the evolution of the volumetric flux with the transmembrane pressure, TMP. In each experiment, the TMP was calculated by subtracting the initial permeate pressure, p_{pi}, from the average feed pressure, p_f:

$$TMP = p_f - p_{pi} \quad (2)$$

Figure 12 shows the steady-state volumetric flux, J, of CO_2 and O_2 as a function of the TMP for all pure PU and PU-based membranes. The results for the PU-based membranes are displayed together with the PU-s membrane because all of them were synthesized using the same solvent content of 35wt%. The pure PU membrane (with no solvent) is also included for comparison.

For every composition, the volumetric flux increases linearly with the TMP and is one order of magnitude greater for CO_2 than for O_2. For both gases, the lowest fluxes were always measured for the pure PU membrane (with no solvent) and the highest fluxes for the PU-s membrane. All the polyurethane-based membranes present with intermediate flux values, always falling in between the PU and PU-s plots for CO_2 and O_2. When comparing the results obtained within the PU-based membranes, the CO_2 flux through the PU/CR membrane is significantly higher than for the PU/TRIS and PU/MBCD membranes. The same tendency is also observed for O_2, albeit to a lesser extent.

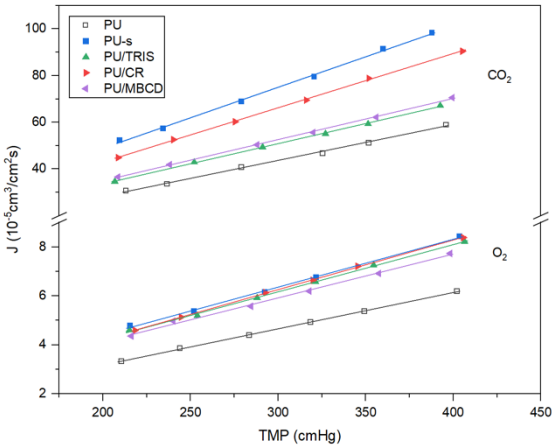

Figure 11. CO_2 and O_2 volumetric fluxes (J) versus the transmembrane pressure (TMP) for the pure polyurethane and polyurethane-based membranes: a) PU, b) PU-s, c) PU/TRIS, d) PU/CR, e) PU/MBCD.

The same analysis was implemented on the data from the permeation curves of CO_2 and O_2 through the mixed matrix membranes. The plots of the volumetric fluxes as a function of the TMP for the PU/Zn-NH_2-BDC, PU/Cu-BTC-0.1 and PU/ Cu-BTC-1.0. are shown in Figure 13. The pure PU membrane is also included in this figure as a reference, since the solvent content in the MMMs is low (10wt%).

The trends observed in this graph are similar to the ones previously described for the other membrane groups. For each composition, the flux values are higher for CO_2 than for O_2 and they increase with the TMP in a linear fashion. All three MMMs present higher fluxes for both gases than the pure PU membrane. For CO_2, the highest flux is seen for the PU/Cu-BTC-0.1 composition, followed by the PU/ Cu-BTC-1.0 and PU/Zn-NH_2-BDC compositions. For O_2, the plots of all three MMMs seem to overlap, and no particular order can be distinguished among them.

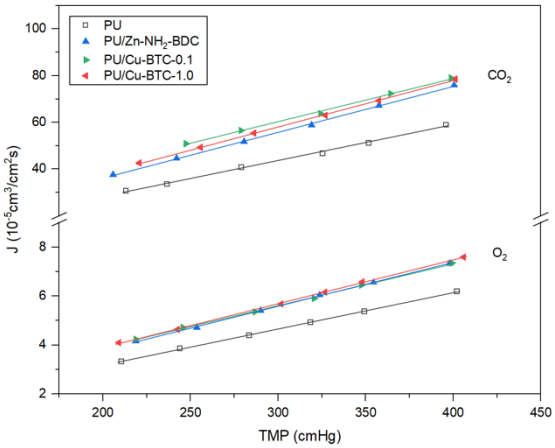

Figure 12. CO_2 and O_2 volumetric fluxes (J) versus the transmembrane pressure (TMP) for the pure polyurethane and mixed matrix membranes: a) PU, b) PU/Zn-NH_2-BDC, c) PU/Cu-BTC-0.1, d) PU/ Cu-BTC-1.0.

One important comment to make is that the flux values are heavily dependent on the membrane thickness: the thinner the membrane, the larger the flux of gas through it. However, these results do not account for the differences in thickness observed in the studied membranes, so further data analysis is necessary to draw meaningful conclusions.

3.5.2. Permeances and permeability coefficients

For every membrane sample, the permeance of each single pure gas, $perm$, can be determined from the slope of its volumetric flux vs. TMP plot:

$$perm = \frac{dJ}{d(TMP)}\left[\frac{cm^3(STP)}{cm^2 s\ cmHg}\right] \quad (3)$$

Since the permeance values depend greatly on the thickness of the membrane, for comparison purposes, it is common to convert them to permeability coefficients, P, which are determined by:

$$P = perm \times \ell \times 10^{10}\ [Barrer] \quad (4)$$

where ℓ is the membrane's thickness [18].

Several (up to six) samples of each composition were tested for each pure gas. The average values, and respective standard deviations, obtained for the permeances and permeability coefficients of CO_2 and O_2 through each studied membrane are reported in Table 3.

From the data shown in Table 3, the same trend can be observed as for the parameters discussed previously, with the permeances and permeability coefficients for all compositions being approximately 10 times higher towards CO_2 than towards O_2. In general, the tendencies observed amongst the permeances of the various compositions are somewhat different from the tendencies observed between the permeability coefficients. This is because the permeability coefficient takes into account the thickness of the membrane and the permeance does not. Since all the membranes have different thicknesses, the P values are more useful for comparison.

Concerning the pure polyurethane membranes from group 1, the P values for CO_2 (P_{CO2}) are higher for the PU-s membrane (278 Barrer) than for the PU membrane (273 Barrer), although the difference is not substantial. However, in the case of O_2, the P values (P_{O2}) are lower for the PU-s membrane (24 Barrer) than for than for the PU membrane (27 Barrer). In terms of oxygen permeation, it seems that the use of solvent during the synthesis of the nonporous PU-s membranes did not provide any advantage.

A composition similar to the PU-s membrane was studied by Eusebio et. al [12] and the P_{CO2} and P_{O2} values found were 227 and 24 Barrer, respectively. Martins [23] also reported P_{CO2} and P_{O2} values of 230 and 22.9 Barrer for pure polyurethane nonporous symmetric membranes synthesized with 35 wt% solvent. Although the P_{O2} values obtained for PU-s in this work were similar to the ones found in previous studies, the P_{CO2} values are considerably higher.

Among the polyurethane-based membranes from group 2, the PU/CR membrane presents the highest values of both P_{CO2} and P_{O2}, at 346 Barrer and 30 Barrer respectively. These values are significantly higher than the ones obtained for the pure polyurethane membranes. On the other hand, the PU/TRIS and PU/MBCD membranes demonstrated lower P_{CO2} values (of 237 and 251 Barrer respectively) than the pure PU membranes. The same P_{O2} value of 26 Barrer was obtained for both these compositions, which in terms of O_2 permeability rank below the PU membrane, but above the PU-s membrane.

In previous research, PU-based membranes with varying quantities (0-15wt%) of polycaprolactone (PCL) were extensively investigated. The P_{CO2} results reported by Faria et. al [8] for PU/PCL membranes, between 113 and 337 Barrer, were comparable to the PU-based membranes studied in this work, but the P_{O2} results were significantly lower, at 10 to 11 Barrer. Improved P_{O2} values of 21 Barrer were obtained by Pon [17] for similar nonporous symmetric membranes PU/PCL membranes, even though the P_{CO2} values were not as high, between 202 and 208 Barrer. Still, all the polyurethane-based membranes investigated in this work presented better O_2 permeability coefficients than in the mentioned previous studies.

All the mixed matrix membranes from group 3 exhibit higher P_{CO2} values than the pure polyurethane membranes, with the PU/Zn-NH_2-BDC membrane (which has 0.1% MOF content) having the highest value of the group (297 Barrer). Within the PU/Cu-BTC membranes, the increase in MOF content from 0.1 wt% to 1.0wt% is accompanied by a decrease of the P_{CO2} value from 287 to 280 Barrer. The highest P_{O2} among the MMM group is found, once again, for the PU/Zn-NH_2-BDC membrane at 27 Barrer, which is approximately the same as the value measured in the PU membrane. A lower P_{O2} value of 26 Barrer was obtained for both PU/Cu-BTC-0.1 and PU/Cu-BTC-1.0 membranes, suggesting that the increase in MOF content had no impact on its O_2 permeability.

It is possible that the increase in Cu-BTC content (from 0.1 to 1.0 wt%) may have contributed to a higher degree of incompatibility between the MOFs and the polyurethane matrix (creating a rigidified region at their interface), causing resistance to the diffusion of permeating species, thus resulting in lower (or unimproved) permeability values for the PU/Cu-BTC-1.0 membrane.

Overall, the novel composition showing the most promising results for the permeation of both CO_2 and O_2 gases is the PU/CR membrane. The PU/TRIS and PU/MBCD membranes seem to provide no improvement to the permeation of either of the studied gases when compared to the pure PU membrane. Regarding the MMMs, although no significant improvement was achieved for the permeation of O_2, the enhanced permeability coefficients found for CO_2 are encouraging.

Furthermore, the results obtained for all the PU membranes in this work represent an improvement when compared to other membrane materials used in current artificial lungs, including Polypropylene (PP) and Polymethylpentene (PMP), which present respective permeability coefficients of 9 and 90 Barrer for CO_2, and 2 and 30 Barrer for O_2 [24]. However, the measurements just mentioned were obtained in a gas/membrane/liquid system, while the experiments in this work were carried out on a gas/membrane/gas system, in which the resistance to gas transport is lower. A more direct comparison could therefore be achieved by repeating the permeation tests done in this work on a gas/membrane/liquid system.

3.5.3. Total surface area required

As described in section 1, the efficient gas exchange in an MBO involves the removal of CO_2 at about 200 cm^3 (STP)/min and delivery of O_2 at approximately 250 cm^3 (STP)/min [3]. The membranes currently used in blood oxygenators commonly have a surface area between 2 to 6 m^2 [24]. Estimations for the surface area required of each membrane to meet these specifications were calculated from the linear flux versus TMP plots exhibited in Figures 12 and 13 (for a feed pressure of 2.0 bar). The values obtained are presented in Table 4

Table 3. Average CO_2 and O_2 permeances (Perm) and permeability coefficients (P) with respective standard deviations for all studied membranes.

Membrane		CO_2 Perm $\left(\frac{10^{-5}cm^3(STP)}{cm^2\ s\ cmHg}\right)$	CO_2 P (Barrer)	O_2 Perm $\left(\frac{10^{-5}cm^3(STP)}{cm^2\ s\ cmHg}\right)$	O_2 P (Barrer)
Group 1	PU	0.151	273 ± 8.5	0.0148	27 ± 1.3
	PU-s	0.251	278 ± 21.4	0.0191	24 ± 2.9
Group 2	PU/TRIS	0.173	237 ± 22.6	0.0193	26 ± 1.2
	PU/CR	0.232	346 ± 25.9	0.0200	30 ± 2.5
	PU/MBCD	0.174	251 ± 17.5	0.0181	26 ± 1.7
Group 3	PU/ Zn-NH_2-BDC	0.196	297 ± 6.5	0.0180	27 ± 0.7
	PU/Cu-BTC-0.1	0.187	287 ± 25.4	0.0171	26 ± 0.7
	PU/Cu-BTC-1.0	0.196	280 ± 4.1	0.0179	26 ± 1.6

Table 4. Volumetric fluxes and estimated required membrane surface areas for all formulations.

Membrane		CO_2 J $\left(\frac{10^{-5} cm^3}{cm^2\ s}\right)$	CO_2 A (m^2)	O_2 J $\left(\frac{10^{-5} cm^3}{cm^2\ s}\right)$	O_2 A (m^2)
Group 1	PU	33.6	1.0	3.9	10.8
	PU-s	57.4	0.6	5.4	7.8
Group 2	PU/TRIS	42.9	0.8	5.2	8.0
	PU/CR	52.6	0.6	5.1	8.1
	PU/MBCD	41.9	0.8	5.0	8.4
Group 3	PU/ Zn-NH_2-BDC	44.6	0.7	4.7	8.8
	PU/Cu-BTC-0.1	50.9	0.7	4.7	8.8
	PU/Cu-BTC-1.0	49.3	0.7	4.6	9.0

As anticipated, higher fluxes of gas across the membranes are correlated to lower required surface areas. In fact, because the fluxes are significantly higher for CO_2 than for O_2, the necessary transfer areas for CO_2 are much lower than for O_2.

The required surface areas obtained in this work ranged from 0.6 to 1.0 m^2 for CO^2 and from 7.8 to 10.8 m^2 for O^2, which represent an improvement when compared to the values reported by Martins [23] for PU/PCL membranes, of 1.2-1.7 m^2 for CO^2 and 13.5-17.5 m^2 for O^2. This is consistent with the enhanced permeability coefficients achieved for CO_2 and O_2 in this work. Nonetheless, the minimum surface areas obtained for oxygen still exceed the range found in membranes for commercial blood oxygenators.

3.5.4. Diffusion and solubility coefficients

Further analysis of the gas permeation measurements, through the time lag method described in section 2.5.2., allowed for the estimation of the diffusion and solubility coefficients for all the studied membranes.

First, the asymptote of the steady state region of the permeation curve is traced. The value at which the steady state asymptote intercepts the x axis (time axis) is defined as the time lag (t_lag). The time lag value and permeability coefficient obtained are then used to determine the D and S coefficients of the membrane, through equations (16) and (1) respectively. This same procedure was applied for all compositions. The values of t_{lag}, D and S obtained for each membrane towards O_2 and CO_2 are displayed in Table 5.

The diffusion coefficients of CO_2 and O_2 presented in Table 5 all have the same order of magnitude and are comparable to the results found in previous studies for PU/PCL membranes, of 1.4x10^{-6} to 1.7x10^{-6} cm^2/s for CO_2, and 1.6x10^{-6} to 2.1x10^{-6} cm^2/s for O_2 [23]. In work by Eusebio et al. [12], higher diffusion coefficients were reported for O_2 than for CO_2, and these findings were justified by the polar character of CO_2 which promotes interactions with the matrix, thus hindering its mobility. However, no clear tendency can be observed in this work regarding which of the two gases presents the highest D values.

When compared to the pure PU and PU-s membranes, the PU/CR membrane shows the highest values of D for both gases. The remaining PU-based membranes, PU/TRIS and PU/MBCD, represent no improvement in the D values for CO_2 but a significant enhancement for the diffusion of O_2 when compared to the pure PU membranes. The MMMs present the most consistent results of all membranes, with slightly higher diffusion coefficients for both gases than the pure PU membranes.

When it comes to the solubility coefficients, the values found for CO_2 are one order of magnitude higher than for O_2 in all membranes. The main parameter influencing the solubility is the ease of condensation [20]. Since carbon dioxide has a higher boiling point than oxygen (-78.5°C and -183 °C, respectively), it is the most likely to condensate. Additionally, the solubility can be correlated to the critical temperature [25]. While the critical point of CO_2 (31.1 °C) is close to the temperature used during the gas permeation experiments (37 °C), O_2 has a negative critical temperature (-118.6 °C) implying that its condensation would not be possible even if the pressure was greatly increased.

Nevertheless, no clear trends can be observed among the solubility values of either gas across the various membranes. In terms of CO_2 solubility, all the pure PU and PU-based membranes exhibit comparable, except for the PU/CR composition which stands out with a lower S value. The O_2 solubility of all PU-based is slightly lower than for the pure PU and PU-s membranes. Once again, the most consistent results are found across the MMMs which present intermediate solubilities values for CO_2 and O_2, with some of the smallest standard deviations. Overall, the solubility coefficients presented in Table 5 are comparable, and even represent a slight improvement, to the values previously reported by Martins [23] for PU/PCL membranes, which ranged from 119.2x10^{-4} to 160.0 x10^{-4} cm^3/cm^3.cmHg for CO_2 and from 9.6x10^{-4} to 11.9 x10^{-4} cm^3/cm^3.cmHg for O_2.

Finally, a combined examination of the coefficients presented in Tables 3 and 5 suggests that the gas permeation through the studied compositions is a diffusion-controlled process, because while no significant trends can be detected among the solubility coefficients, the tendencies observed among the diffusion coefficients are identical to the ones observed in the permeability coefficients.

4. Conclusions

The carbon dioxide (CO_2) and oxygen (O_2) gas permeation properties of novel polyurethane-based dense membranes were studied in this work. From the permeate pressure vs. time curves, obtained from experiments at multiple feed pressures, it was possible to plot the steady state gas flux (J) as a function of the transmembrane pressure (TMP), thus determining the permeability, diffusion and solubility coefficients of each membrane.

Three groups of nonporous symmetric membranes were prepared by the solvent evaporation technique: pure polyurethane, polyurethane-based and mixed matrix membranes (MMMs). The pure polyurethane membranes, PU and PU-s, were obtained from casting solutions of polyurethane (PU) with and without dimethylformamide (DMF) as the solvent. The polyurethane-based membranes, PU/TRIS, PU/CR and PU/MBCD, were prepared from casting solutions of PU and DMF with tris(hydroxymethyl) aminomethane (TRIS), Congo red (CR) and methyl-beta-cyclodextrin (MBCD). Finally, the MMMs, PU/Zn-NH2-BDC, PU/Cu-BTC-0.1 and PU/Cu-BTC-1.0, were synthesized by incorporating Zn-NH2-BDC and Cu-BTC metal organic frameworks (MOFs) into casting solutions of PU and DMF.

Table 5. Time lag values (t_{lag}) diffusion coefficients (D) and solubility coefficients (S) obtained from the O_2 and CO_2 permeation curves for all the studied membranes.

Membrane		CO_2 t_{lag} (s)	CO_2 D $\left(\frac{10^{-6} cm^2}{s}\right)$	CO_2 S $\left(\frac{10^{-4} cm^3}{cm^3 cmHg}\right)$	O_2 t_{lag} (s)	O_2 D $\left(\frac{10^{-6} cm^2}{s}\right)$	O_2 S $\left(\frac{10^{-4} cm^3}{cm^3 cmHg}\right)$
Group 1	PU	37.2	1.5 ± 0.1	185.5 ± 9.6	27.4	2.0 ± 0.2	13.4 ± 1.0
	PU-s	11.5	1.8 ± 0.4	154.6 ± 26.9	18.2	1.5 ± 0.3	16.6 ± 3.2
Group 2	PU/TRIS	22.2	1.4 ± 0.2	168.3 ± 22.8	14.7	2.2 ± 0.4	12.3 ± 1.7
	PU/CR	12.4	3.1 ± 0.6	114.5 ± 15.2	14.7	2.6 ± 0.6	11.7 ± 1.8
	PU/MBCD	25.6	1.5 ± 0.4	183.0 ± 50.9	15.3	2.3 ± 0.4	11.4 ± 1.6
Group 3	PU/ Zn-NH_2-BDC	18.6	2.1 ± 0.1	144.3 ± 4.7	212	1.8 ± 0.1	15.0 ± 0.3
	PU/Cu-BTC-0.1	21.0	1.9 ± 0.2	153.6 ± 25.2	20.4	1.9 ± 0.1	13.6 ± 0.4
	PU/Cu-BTC-1.0	18.1	1.9 ± 0.2	149.6 ± 16.8	19.9	1.7 ± 0.2	14.9 ± 0.9

The SEM images revealed that all membranes present a homogenous, dense cross-section with no visible pores. It appears that the addition of TRIS, CR and MBCD did not have any effect on the membrane morphology when compared to the pure PU membranes. The cross-section images of the PU/Zn-NH2-BDC and PU/Cu-BTC-1.0 membranes showed the presence of small features which distinguished themselves from the polyurethane matrix. An EDS analysis of these membranes confirmed that the observed features were in fact Zn-NH2-BDC and Cu-BTC (MOFs), respectively.

The average thickness of each membrane was obtained from the cross-sectional SEM images. The highest thickness (181 µm) was obtained for the PU membrane, and the lowest for the PU-s membrane (125 µm). All of the PU-based membranes and MMMs exhibited intermediate thickness ranging from 137 to 149 µm and 143 to 152 µm, respectively. It was found that casting solutions with higher solvent content resulted in membranes of lower thickness.

All the studied membranes, as well as the PU prepolymer, were analyzed through ATR – FTIR spectroscopy. The spectra of all membranes exhibited the urethane/urea carbonyl stretching band at about 1730 cm^{-1}, but none presented a peak centered at 2278 cm^{-1}, corresponding to the asymmetric isocyanate stretching mode (uasNCO), which is observable in the PU prepolymer spectrum. This implies that all the isocyanate groups probably reacted with the functional groups of the components present in the PU-based membranes (TRIS, CR and MBCD).

All the stress-strain curves obtained from the tensile tests carried out on the pure polyurethane and polyurethane-based membranes were similar in shape, exhibiting a behavior typical of elastomers. The initial Young's modulus, tensile strength and elongation at break were in the ranges of 2.3-8.0 MPa, 1.5-2.7 MPa, and 78.70-116.35%, respectively. The pure PU membrane presented the highest elasticity modulus and tensile strength, and the PU/CR membrane had the highest elongation at break.

The pure PU and PU-s membranes exhibited permeability coefficients of 273 and 278 Barrer towards CO_2, and 27 and 24 Barrer towards O_2, respectively, For the PU-based membranes, CO_2 permeabilities of 237, 346, and 251 Barrer and O_2 permeabilities of 26, 30 and 26 Barrer were obtained for PU/TRIS, PU/CR and PU/MBCD, respectively. Regarding the MMMs, P values of 297, 287, 280 Barrer towards CO_2 and 27, 26 and 26 Barrer towards O_2 were found for PU/Zn-NH2-BDC, PU/Cu-BTC-0.1 and PU/Cu-BTC-1.0, respectively.

All the P_{CO2} values are one order of magnitude greater than the P_{O2} values. When compared to the pure PU membranes, the composition that represents the biggest improvements in terms of CO_2 and O_2 permeabilities was PU/CR, followed by PU/Zn-NH2-BDC and PU/Cu-BTC-0.1. The PU/TRIS and PU/MBCD membranes present some of the lowest permeability values, particularly for CO_2, suggesting that the addition of TRIS and MBCD does not bring any enhancement to the performance of the pure PU membrane. Furthermore, the increased MOF content in the PU/Cu-BTC-1.0 membrane does not yield improved permeation of either gas in relation to the PU/Cu-BTC-0.1 membrane. The great fluxes of CO_2 observed through the studied membranes resulted in estimated minimum membrane surface areas ranging from 0.6 to 1.0 m^2, which compares favorably to the membrane areas used in current commercial MBO of approximately $2m^2$. However, the surface area requirements estimated from the O_2 fluxes, 7.8 to 10.8 m^2, still exceed the areas found in commercial MBOs. This indicates that the O2 permeation properties are a limiting factor.

The diffusion coefficient ranges calculated through the time-lag method were $1.4x10^{-6}$-$3.1x10^{-6}$ cm^2/s for CO_2, and $1.5x10^{-6}$-$2.6x10^{-6}$ cm^2/s for O_2. These results followed the same trends observed for the permeability coefficients, with PU/CR having the highest value, followed by the MMMs, and with PU/TRIS and PU/MBCD exhibiting the lowest values. On the other hand, the solubility coefficients found ranged from $114.5x10^{-4}$ to $185.5x10^{-4}$ $cm^3/cm^3.cmHg$ for CO_2, and 11.4 $x10^{-4}$ to $16.6x10^{-4}$ $cm^3/cm^3.cmHg$ for O_2. All the solubility values were within the same order of magnitude and no significant tendencies could be observed among them. From these results, the permeation process of the respiratory gases through the studied membranes appears to be controlled by diffusion.

5. Bibliography

[1] Kapoor PM, Navin C Nanda. Manual of Extracorporeal Membrane Oxygenation (ECMO) in the ICU. First edition. Jaypee Brothers Medical Publishers (P) Ltd.; 2014.

[2] MacLaren G, Combes A, Bartlett RH. Contemporary extracorporeal membrane oxygenation for adult respiratory failure: life support in the new era. Intensive Care Medicine 2012;38:210–20.

[3] Stamatialis DF, Papenburg BJ, Gironés M, Saiful S, Bettahalli SNM, Schmitmeier S, et al. Medical applications of membranes: Drug delivery, artificial organs and tissue engineering. Journal of Membrane Science 2008;308:1–34.

[4] Wiese F. Membranes for Artificial Lungs. Membranes for the Life Sciences, Weinheim, Germany: Wiley-VCH Verlag GmbH & Co. KGaA; 2010, p. 49–68.

[5] Meyns B, Vercaemst L, Vandezande E, Bollen H, Vlasselaers D. Plasma Leakage of Oxygenators in ECMO Depends on the Type of Oxygenator and on Patient Variables. The International Journal of Artificial Organs 2005;28:30–4.

[6] Faria M, Brogueira P, de Pinho MN. Sub-micron tailoring of bi-soft segment asymmetric polyurethane membrane surfaces with enhanced hemocompatibility properties. Colloids and Surfaces B: Biointerfaces 2011;86:21–7.

[7] Applications B, Mostafavi AH, Kumar Mishra A, Ulbricht M, Denayer JFM, Hosseini SS. Oxygenation and Membrane Oxygenators: Emergence, Evolution and Progress in Material Development and Process Enhancement for Article info. Journal of Membrane Science and Research 2021;7:230–59.

[8] Faria M, de Pinho MN. Phase segregation and gas permeation properties of poly(urethane urea) bi-soft segment membranes. European Polymer Journal 2016;82:260–76.

[9] Besteiro MC, Guiomar AJ, Gonçalves CA, Bairos VA, de Pinho MN, Gil MH. Characterization and in vitro hemocompatibility of bi-soft segment, polycaprolactone-based poly(ester urethane urea) membranes. Journal of Biomedical Materials Research - Part A 2010;93:954–64.

[10] Zhao C-T, Norberta De Pinho M. Design of polypropylene oxide/polybutadiene bi-soft segment urethane/ urea polymer for pervaporation membranes. Polymer (Guildf) 1998;40:6089–97.

[11] Queiroz DP, de Pinho MN. Structural characteristics and gas permeation properties of polydimethylsiloxane/poly(propylene oxide) urethane/urea bi-soft segment membranes. Polymer (Guildf) 2005;46:2346–53.

[12] Eusébio TM, Martins AR, Pon G, Faria M, Morgado P, Pinto ML, et al. Sorption/diffusion contributions to the gas permeation properties of bi-soft segment polyurethane/polycaprolactone membranes for membrane blood oxygenators. Membranes (Basel) 2020;10.

[13] Faria M, Rajagopalan M, de Pinho MN. Tailoring bi-soft segment poly (ester urethane urea) integral asymmetric membranes for CO2 and O2 permeation. Journal of Membrane Science 2012;387–388:66–75. https://doi.org/10.1016/j.memsci.2011.10.010.

[14] Wang H, Zhao S, Liu Y, Yao R, Wang X, Cao Y, et al. Membrane adsorbers with ultrahigh metal-organic framework loading for high flux separations. Nature Communications 2019;10.

[15] Somarathna HMCC, Raman SN, Mohotti D, Mutalib AA, Badri KH. Rate dependent tensile behavior of polyurethane under varying strain rates. Construction and Building Materials 2020;254.

[16] Eusébio TM. Polyurethane urea membranes for membrane blood oxygenators: synthesis and gas permeation properties. Master of Science. Instituto Superior Tecnico, 2017.

[17] Pon G. Gas permeation in bi-soft segment poly(ester urethane urea) membranes for Membrane Blood Oxygenators. Master of Science. Instituto Superior Tecnico, 2018.

[18] Ismail AF, Chandra Khulbe K, Matsuura T. Gas Separation Membranes: Polymeric and Inorganic. Cham: Springer International Publishing; 2015.

[19] Park GS. Transport Principles—Solution, Diffusion and Permeation in Polymer Membranes. Synthetic Membranes: Science, Engineering and Applications, Dordrecht: Springer Netherlands; 1986, p. 57–107.

[20] Mulder M. Basic Principles of Membrane Technology. 2nd Edition. Kluwer Academic Publishers; 1996.

[21] Barrer RM, Rideal EK. Permeation, diffusion and solution of gases in organic polymers. Trans Faraday Soc 1934:628–43.

[22] Wallace WE. Carbon dioxide. NIST Mass Spectrometry Data Center n.d. https://webbook.nist.gov/cgi/inchi?ID=C124389&Type=IR-SPEC&Index=0 (accessed May 28, 2022).

[23] Gonçalves Varandas Martins AR. Characterization and Gas Permeation Properties of Blood Compatible Membranes for Blood Oxygenators. Master of Science. Instituto Superior Tecnico, 2019.

[24] Gray DN. Polymeric Membranes for Artificial Lungs. Polymeric Materials and Artificial Organs, 1984, p. 151–62.

[25] Baker RW, Low BT. Gas separation membrane materials: A perspective. Macromolecules 2014;47:6999–7013.